iScience

CellPress
OPEN ACCESS

Article

Adipose tissue plasticity in pheochromocytoma patients suggests a role of the splicing machinery in human adipose browning

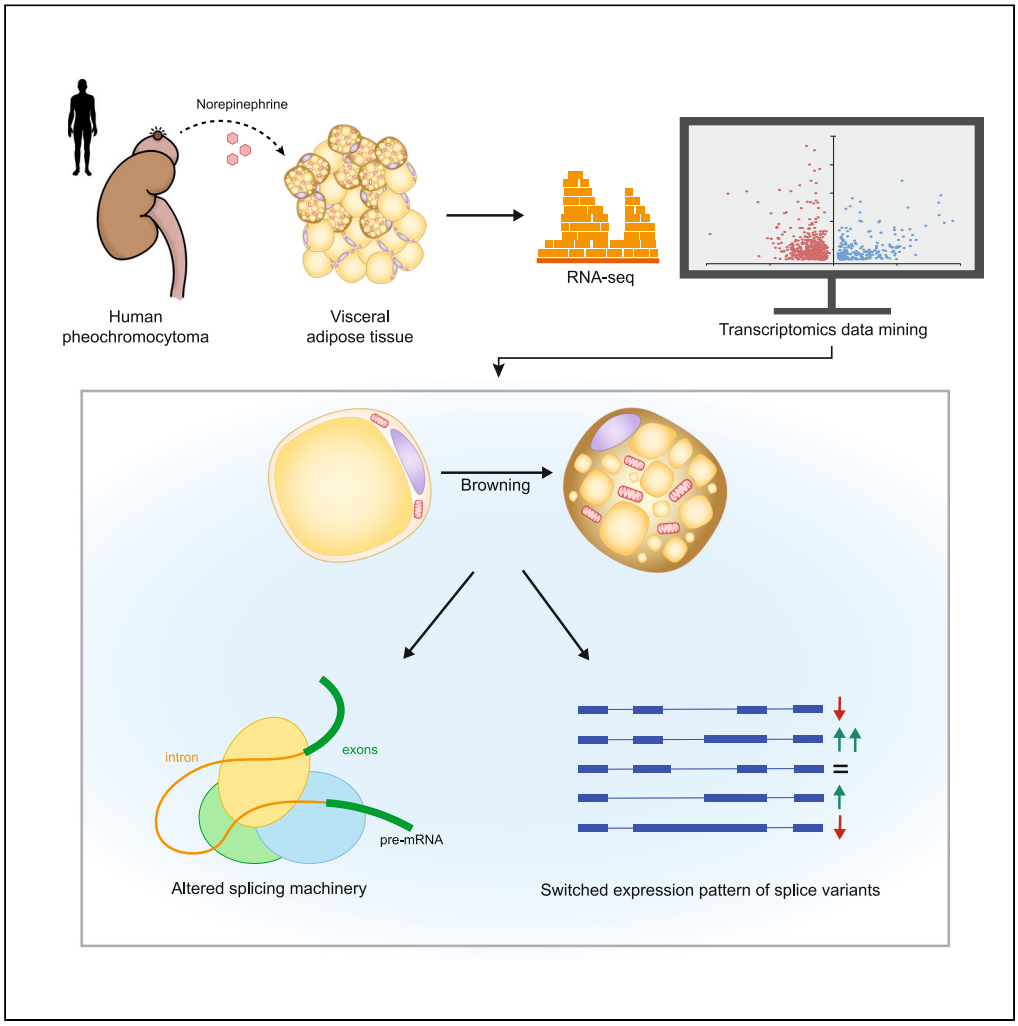

Moisés Castellá, Albert Blasco-Roset, Marion Peyrou, ..., Décio L. Eizirik, Francesc Villarroya, Rubén Cereijo

fvillarroya@ub.edu (F.V.)
rcereijo@ub.edu (R.C.)

Highlights

Adipose tissue from patients with pheochromocytoma acquires a beige fat phenotype

Transcriptomics of this human adipose browning model is assessed for the first time

Massive regulation of splicing machinery occurs in human browning and beige cells

Isoform pattern changes suggest a relevant role for splicing in human browning

Castellá et al., iScience 26, 106847
June 16, 2023
https://doi.org/10.1016/j.isci.2023.106847

iScience

CellPress
OPEN ACCESS

Article

Adipose tissue plasticity in pheochromocytoma patients suggests a role of the splicing machinery in human adipose browning

Moisés Castellá,[1,2,11] Albert Blasco-Roset,[1,2,11] Marion Peyrou,[1,2] Aleix Gavaldà-Navarro,[1,2] Joan Villarroya,[1,2] Tania Quesada-López,[1,2,3] Leyre Lorente-Poch,[4] Juan Sancho,[4] Florian Szymczak,[5,6] Anthony Piron,[5,6] Sonia Rodríguez-Fernández,[7] Stefania Carobbio,[8] Albert Goday,[2,9,10] Pere Domingo,[3,10] Antonio Vidal-Puig,[7] Marta Giralt,[1,2] Décio L. Eizirik,[5] Francesc Villarroya,[1,2,*] and Rubén Cereijo[1,2,3,12,*]

SUMMARY

Adipose tissue from pheochromocytoma patients acquires brown fat features, making it a valuable model for studying the mechanisms that control thermogenic adipose plasticity in humans. Transcriptomic analyses revealed a massive downregulation of splicing machinery components and splicing regulatory factors in browned adipose tissue from patients, with upregulation of a few genes encoding RNA-binding proteins potentially involved in splicing regulation. These changes were also observed in cell culture models of human brown adipocyte differentiation, confirming a potential involvement of splicing in the cell-autonomous control of adipose browning. The coordinated changes in splicing are associated with a profound modification in the expression levels of splicing-driven transcript isoforms for genes involved in the specialized metabolism of brown adipocytes and those encoding master transcriptional regulators of adipose browning. Splicing control appears to be a relevant component of the coordinated gene expression changes that allow human adipose tissue to acquire a brown phenotype.

INTRODUCTION

Adipose depots in mammals, including humans, have traditionally been classified as white adipose tissue (WAT), which contains energy-storing white adipocytes, and brown adipose tissue (BAT), which contain thermogenic brown adipocytes. Brown adipocytes express uncoupling protein-1 (UCP1), which confers specific thermogenic properties to mitochondria, and possess enzymatic machinery that enables the rapid oxidation of metabolic substrates to sustain thermogenesis. The distinction between the energy-storing properties of WAT and the energy-spending (thermogenic) features of BAT has reciprocal implications for metabolism: WAT accumulation is linked to obesity and associated diseases, such as diabetes and hyperlipidemia, whereas BAT activation protects against these conditions.[1] In recent years, researchers have recognized the remarkable plasticity of adipose tissue, especially in the capacity of adipose depots anatomically defined as WAT to acquire thermogenic properties via the recruitment of thermogenic brown-like adipocytes (called beige or brite cells).[2] Beige adipocytes develop from a cell lineage distinct from that leading to the classical brown adipocytes present in BAT depots[3] but share with them the capacity to undergo adaptive heat production via both UCP1 expression and the associated uncoupling of mitochondrial respiration,[4] and additional non-UCP1-mediated thermogenic mechanisms.[5] The process through which a fat depot is enriched for beige cells is called the browning of adipose tissue. In rodent models, browning is activated in response to thermogenic stimuli, such as exposure to a cold environment.[2,6] The induction of browning is mainly mediated through β-adrenergic stimulation, although it may be influenced by other hormones and by pharmacological agents.[7,8] β-adrenergic stimulation not only activates thermogenesis in existing brown or beige adipocytes but also promotes browning in former WAT depots. Accumulating evidence suggests that the capacity to activate the browning process is associated with protection against diet-induced obesity in experimental rodent models.[9]

Humans and other mammals possess BAT depots; although it was long believed that active BAT was restricted to the neonatal and early infancy periods in humans, researchers eventually recognized that

Continued

[1]Departament de Bioquímica i Biomedicina Molecular, Universitat de Barcelona; Institut de Biomedicina de la Universitat de Barcelona (IBUB); and Institut de Recerca de Sant Joan de Déu, 08028 Barcelona, Spain

[2]CIBER Fisiopatología de la Obesidad y Nutrición, 28029 Madrid, Spain

[3]Institut d'Investigació Biomèdica Sant Pau (IIB SANT PAU), Hospital de la Santa Creu i Sant Pau, and Department of Infectious Diseases, Hospital de la Santa Creu i Sant Pau, 08041 Barcelona, Spain

[4]Endocrine Surgery Unit, Hospital del Mar, 08003 Barcelona, Spain

[5]ULB Center for Diabetes Research, Medical Faculty, Université Libre De Bruxelles (ULB), 1070 Brussels, Belgium

[6]Interuniversity Institute of Bioinformatics in Brussels, Université Libre de Bruxelles-Vrije Universiteit Brussel, 1050 Brussels, Belgium

[7]University of Cambridge Metabolic Research Laboratories, Wellcome-MRC Institute of Metabolic Science, Addenbrooke's Hospital, Cambridge 289, UK

[8]Bases Moleculares de Patologías Humanas, Centro de Investigación Príncipe Felipe, 46012 Valencia, Spain

[9]Endocrinology Service, Hospital del Mar, IMIM, 08003 Barcelona, Spain

[10]Department of Medicine, Universitat Autònoma de Barcelona, 08193 Cerdanyola del Vallès, Spain

[11]These authors contributed equally

active BAT persists in adult humans.[10] Analyses of adipose depots presenting thermogenic BAT-like activity in adult humans indicate cellular heterogeneity and an abundant presence of cells characteristic of the beige adipocyte lineage.[11] Understanding the mechanisms and regulation of adipose tissue browning in humans is of utmost relevance, given that high brown/beige activity is associated with protection against obesity, type II diabetes, and cardiovascular disease in adult humans.[12]

The potential browning capacity of human adipose tissue was first recognized decades ago when it was reported that adipose tissue in the vicinity of pheochromocytoma tumors could acquire BAT-like features.[13,14] In omental adipose depots from patients with pheochromocytoma, cells showing multilocular lipid droplets and expressing UCP1 appear interspersed with other unilocular adipocytes and exhibit gene expression and mitochondrial respiratory features typical of thermogenic brown/beige adipocytes.[15–19] It is implied that the intense secretion of catecholamines by the tumor creates a local environment reminiscent of sustained β-adrenergic stimulation of adipose depots, which elicits the browning process.[20]

The study of adipose tissue browning in response to pheochromocytoma-elicited stimulation allows researchers to circumvent the difficulties of experimentally analyzing browning in response to chronic and intense beta-adrenergic stimuli in humans. Using adipose tissue samples from pheochromocytoma patients, researchers have studied the cellular lineage, endocrine role, mitochondrial remodeling, and other processes of human beige adipose tissue, and compared their results with those obtained from the much more easily accessible experimental rodent models.[16,18,21]

Here, we used massive and non-biased deep transcriptomics analyses of adipose tissue from pheochromocytoma patients to shed new light on the actual processes involved in browning adipose tissue in humans. Our results suggest regulated splicing as a potentially relevant process associated with human adipose browning.

RESULTS

Evidence of browning in adipose tissue from pheochromocytoma patients

Visceral adipose samples obtained during surgical ablation of pheochromocytoma tumors were analyzed for morphological evidence of browning using electron transfer microscopy. RNA prepared from the adipose samples was analyzed for the expression of genes known to be preferentially expressed in brown/beige adipocytes (*UCP1; CKMT1A* and *CKMT1B*, encoding creatine kinase, mitochondrial 1A and 1B) or white adipocytes *(LEP*, leptin) in comparison with a set of samples of visceral adipose tissue from age-matched control, non-pheochromocytoma, patients. Adipose samples from different pheochromocytoma patients consistently exhibited scattered clusters of characteristic brown/beige adipocytes, identified by their multilocular distribution of lipid droplets and high density of mitochondria (see representative examples in Figure 1A). The expression of *UCP1*, which is characteristic of brown and beige adipocytes but absent from white adipocytes, was observed in all adipose samples from pheochromocytoma patients but was almost undetectable in control samples (Figure 1B). The expression levels of *CKMT1A* and *CKMT1B*, which are enhanced in brown/beige cells,[22] were also much higher in adipose samples from patients relative to controls. Leptin expression showed a reciprocal expression pattern: it was higher in control adipose tissue than in pheochromocytoma patients. The expression levels of *UCP1*, *CKMT1A* and *CKMT1B* differed among individual samples, likely reflecting between-patient differences in the extent of browning.

Transcriptomics analysis of differentially expressed genes in adipose tissue from pheochromocytoma patients

We next determined, in a non-biased manner, the whole-transcriptome changes associated with the browning of human adipose tissue; we chose the four adipose tissue samples from pheochromocytoma patients that showed the most overt evidence of browning and the three samples of adipose tissue from healthy controls that exhibited the most pronounced features of WAT. We performed RNA-sequencing (RNA-seq) analysis and calculated each sample's relative whole-genome transcript levels. Whole genome analysis of transcript patterns across samples was performed using principal component analysis (PCA). The results revealed that the samples could be clearly separated between patients (browned) and controls based on their overall transcript patterns (Figure S1).

[12]Lead contact

*Correspondence:
fvillarroya@ub.edu (F.V.),
rcereijo@ub.edu (R.C.)

https://doi.org/10.1016/j.isci.2023.106847

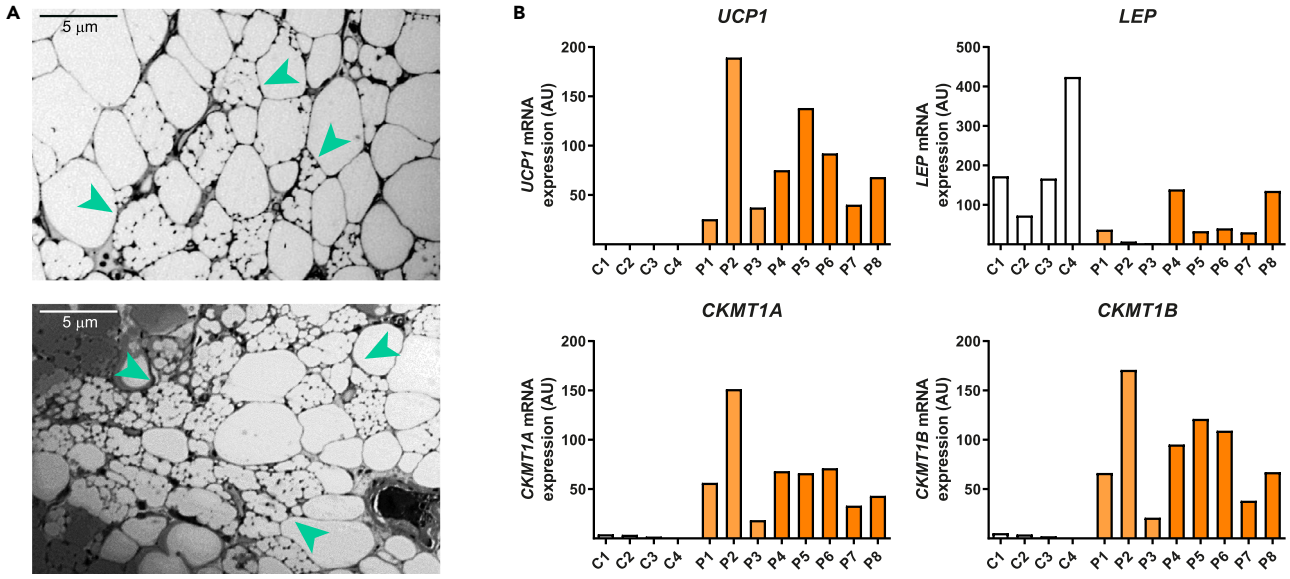

Figure 1. Evidence of browning in adipose tissue from individuals with pheochromocytoma

(A) Representative transmission electron microscopy pictures of adipose tissue from the omental region of two pheochromocytoma patients (upper: 50-year-old male, lower: 41-year-old female). Scale bars represent 5 µm. Arrows indicate multilocular beige adipocytes.

(B) *UCP1*, *CKMT1A*, *CKMT1B*, and *LEP* mRNA expression levels in adipose samples from individuals with pheochromocytoma (P1-8) and healthy controls (C1-4). See also Figure S1.

Figure 2A shows a volcano plot representation of genes differentially expressed in adipose tissue from pheochromocytoma patients versus controls. When we used a threshold of 1.5 fold-change (FC) (i.e., $\log_2(FC) = 0.585$) and significance of $p<0.05$ to compare gene transcript levels, our results revealed that 242 genes were up-regulated and 503 genes were down-regulated in patients versus controls (for a complete list of significantly differentially expressed transcripts see Table S1).

These results from our transcriptome analysis confirmed the upregulation of *UCP1*, *CKMT1A*, and *CKMT1B*, as previously assessed by qRT-PCR (Figure 1B). Other genes related to the brown/beige adipose phenotype, such as *DIO2* and *PPARGC1A*,[6] were also induced in adipose tissues of pheochromocytoma patients. Other transcripts remarkably up-regulated in patients included genes involved in lipid and oxidative catabolism, such as: *PNPLA4*, encoding a phospholipase of the same patatin-like family as adipose triglyceride lipase (ATGL), a key enzyme for lipolysis; *ELOVL6*, which encodes a very long chain fatty acid elongase critical for adipocyte thermogenic activation[23]; and *OGDHL*, which encodes the tricarboxylic acid cycle component, 2-oxoglutarate dehydrogenase. The transcript levels of *PCK1*, encoding phosphoenolpyruvate carboxykinase, were also up-regulated in the browned adipose tissue. This agrees with previous reports indicating that *PCK1* mRNA is preferentially expressed in BAT versus WAT[24] and an early induced gene in human brown adipogenic differentiation.[25] The previous findings in brown/beige adipocytes and their precursors are therefore consistent with the present transcriptomics analysis on adipose tissue from pheochromocytoma patients.

Differentially expressed transcripts in pheochromocytoma versus control adipose samples were analyzed using BATLAS, an algorithm that uses transcript expression data to calculate the brown adipocyte content of complex human biopsies.[26] The results confirmed the acquisition of a significant brown-versus-white phenotype in the pheochromocytoma patients (Figure S2A). An additional analysis comparing the pheochromocytoma-versus-control transcriptome with a database of the differential transcriptome of human deep-neck BAT versus WAT[27] also showed a significant induction of a brown-type phenotype in the pheochromocytoma samples (Figure S2B).

Functional enrichment analyses (Figure 2B, Table S2) using KEGG revealed that the most significantly up-regulated pathways in adipose samples from pheochromocytoma patients were those related to metabolism, including fatty acid and carbohydrate metabolism, and associated regulatory processes, such as

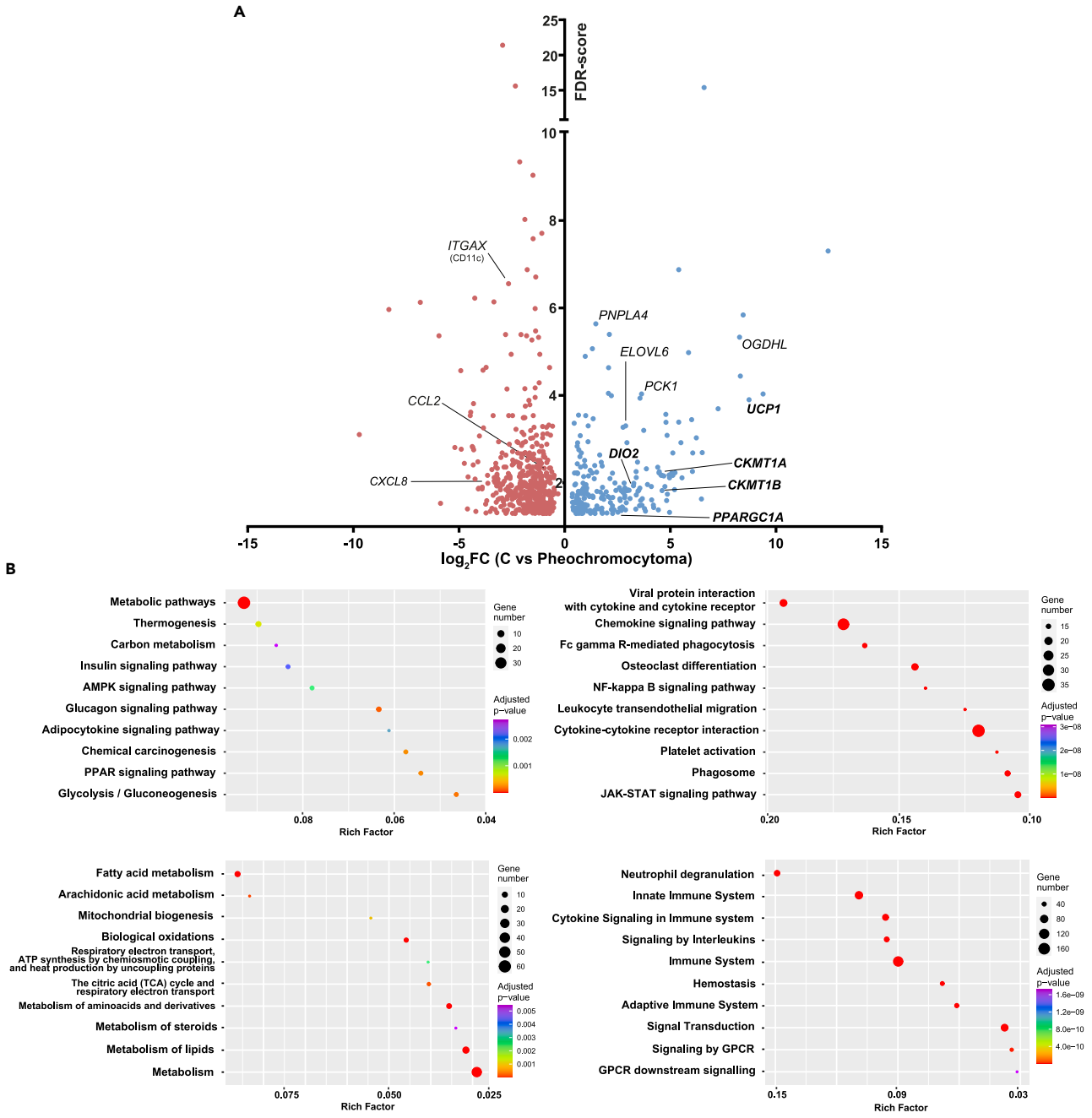

Figure 2. Transcriptomics analysis of differentially expressed genes in adipose tissue from pheochromocytoma patients

(A) Volcano plot depicting significantly up-regulated or down-regulated transcripts in adipose tissue samples from individuals with pheochromocytoma (N = 4) versus healthy controls (N = 3). The criteria for statistical significance were a false discovery rate (FDR) > 1.3 (pvalue <0.05) and $\log_2$ of fold change (FC) > | 0.585| (1.5-fold). Transcripts corresponding to markers of brown/beige adipose tissue and inflammation are indicated.

(B) Enrichment scatter diagrams showing the top-10 most highly altered pathways according to KEGG (top panels) and REACTOME (down panels) database analysis of the up-regulated (left) and down-regulated (right) transcripts in adipose tissue from pheochromocytoma patients relative to controls. The vertical axis represents the pathway name and the horizontal axis the rich factor corresponding to the pathway. Significant differences are indicated by pvalue ($p < 0.05$). The magnitude of the pvalue is represented by the dot color and the number of DEGs (differentially expressed genes) within each pathway is indicated by the dot size. See also Figure S2 and Tables S1 and S2.

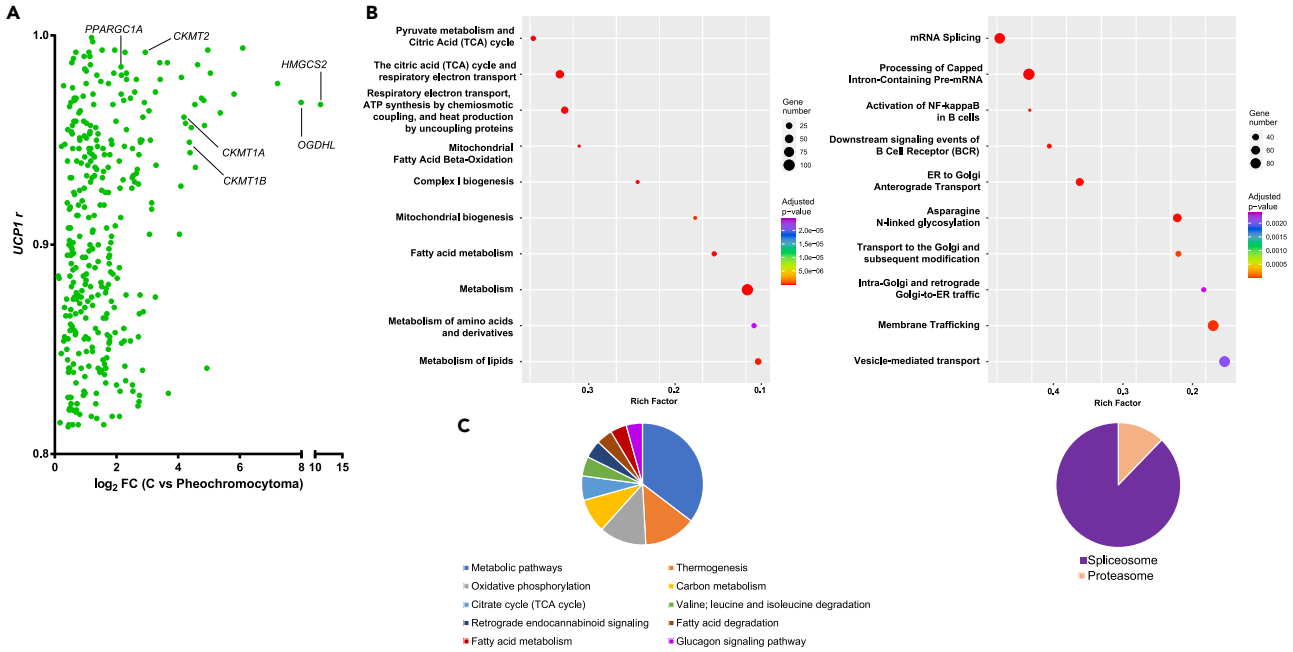

Figure 3. Profile of genes associated with *UCP1* expression in human adipose tissue

(A) Dispersion plot depicting transcripts positively correlated with uncoupling protein 1 (*UCP1*) transcript levels in the whole dataset ($N = 7$) in terms of Pearson's correlation coefficient (r) and $\log_2$ of fold change (FC) in pheochromocytoma samples as compared to respective controls; r and $\log_2$(FC) pvalues <0.05 were used as the threshold for statistical significance.

(B) Enrichment scatter diagrams showing the top-10 most highly altered pathways according to REACTOME database analysis of the statically significant ($p < 0.05$) transcripts positively-correlated (left) and negatively-correlated (right) with UCP1 mRNA expression in adipose tissue from controls and pheochromocytoma patients ($N = 7$). The vertical axis represents the pathway name and the horizontal axis the rich factor corresponding to the pathway. Significant differences are indicated by $p < 0.05$. The magnitude of the p-value is represented by the dot color and the number of UCP1-correlated genes within each pathway is indicated by the dot size.

(C) Pie chart representation of the top-scoring pathways corresponding to statistically significant ($p < 0.05$) positively-correlated (left) and negatively-correlated (right) with UCP1 mRNA expression in adipose tissue from controls and pheochromocytoma patients ($N = 7$) according to the KEGG database analysis.

signaling involving insulin, AMP kinase, and PPARs. This non-biased analysis also detected thermogenesis as a significantly induced pathway (Figure 2B). An additional analysis using REACTOME confirmed the increased prevalence of metabolic pathways and mitochondria-uncoupled respiration in adipose samples from the pheochromocytoma patients (Figure 2B). Overall, our analyses confirmed that the adipose samples of pheochromocytoma patients showed the induction of thermogenic and oxidative lipid metabolism typical of browning.

Of interest, our analysis of the down-regulated gene pathways revealed a totally different scenario. Both KEGG and REACTOME analyses of the down-regulated pathways identified the downregulation of immune system-related processes (Figure 2B, right). Inflammation/immune pathways such as "chemokine signaling pathway" and "cytokine-cytokine receptor interaction, innate and cytokine signaling in immune systems" were identified as the most highly down-regulated pathways (see the pro-inflammatory markers, *ITGAX*/CD11c, *CCL2* and *CXCL8*, in Figure 2A). This finding is consistent with experimental findings in rodent models suggesting that the downregulation of inflammation-related pathways and cross-talk between immune cells and adipogenic cells are involved in adipose tissue plasticity and browning.[28]

Gene expression profile associated with *UCP1* expression in human adipose tissue

The analysis described above indicated that the adipose samples from pheochromocytoma patients showed morphological and molecular evidence of browning. We observed, however, remarkable variability in the extent of brown/beige adipocyte content, based on the expression of the "gold-standard" marker gene, *UCP1*. We used this variability to determine in a non-biased manner which pathways were

the most highly associated with the extent of browning. Our analysis revealed that 749 and 2894 transcripts correlated positively and negatively with *UCP1* mRNA levels, respectively (see Table S3). Figure 3A shows the Pearson correlations of the transcript levels of various genes with that of *UCP1* in the samples analyzed. The top correlated transcripts included expected genes such as *CKMT1A*, *CKMT1B* and *CKMT2*, which encode components of the creatine kinase-related pathways that appear to contribute to thermogenesis in beige cells,[5] and *PPARGC1A*, which encodes the master co-transcriptional regulator of brown/beige adipogenesis, PGC-1α.[29] Of interest, *HGMCS2*, which encodes hydroxymethylglutaryl-coenzyme A synthase 2, was the top transcript correlated with the *UCP1* mRNA level, which is consistent with previous findings that identified *HMGCS2* as the top-induced lipid metabolism gene in the cold response of supraclavicular human BAT.[30]

In addition, we conducted an enrichment analysis using REACTOME and KEGG to determine the pathways and processes significantly associated with the overall transcripts pattern of genes whose mRNA levels correlated with that of *UCP1* (Figure 3, Table S4). The top REACTOME-identified pathways (Figure 3B, left) included "metabolism" followed by several mitochondrial metabolism-related pathways and processes (respiratory chain, TCA cycle, mitochondrial biogenesis, mitochondrial fatty acid oxidation, etc.). The KEGG analysis (see Figure 3C, left, for a pie chart representation of the top 10 pathways) confirmed that "thermogenesis" correlated with the extent of *UCP1* expression, as did oxidative phosphorylation- and TCA cycle-related metabolic pathways and fatty acid catabolism. These findings agreed with above-described pathway analysis and indicated that mitochondrial biogenesis and mitochondrial metabolism processes are directly associated with the extent of browning in adipose tissue. This is consistent with the known intrinsic enrichment of the mitochondrial oxidative machinery in brown/beige adipocytes.[6]

Of interest, our REACTOME-based analysis of the top pathways that were negatively associated with the extent of *UCP1* expression in adipose samples (Figure 3B, right) identified splicing-associated processes of capped-intron containing pre-mRNA", "mRNA splicing") and pathways related to intracellular and extracellular protein trafficking. Moreover, KEGG analysis (pie chart in Figure 3C, right) revealed marked negative associations between *UCP1* expression and "spliceosome" and (to a lesser extent) "proteasome".

Downregulation of splicing factors and splicing-related proteins in association with browning

The potential involvement of splicing processes in browning prompted us to check the expression levels of transcripts encoding components of the splicing machinery and its regulation. Figure 4A shows the expression levels of 47 representative splicing-related factors, selected according to the SpliceAid dataset,[31] in adipose tissues from pheochromocytoma patients relative to controls. These data confirmed a massive trend for downregulation of splicing-related factors in browned samples (significant decreases in 35 of 47 analyzed factors and non-significant decreasing trends in many others). The down-regulated factors included those involved in forming the pre-mRNP and spliceosomal complexes A, C, and E, as well as components of the exon inclusion/exclusion machinery. Exceptions to this global downregulation of the splicing machinery were the significant upregulation of *ELAVL3* and *ELAVL4* (encoding two RNA-binding proteins involved in regulating alternative splicing[32]), and non-significant trends for upregulation of *PRPF8* and *RBFOX1* in the pheochromocytoma adipose tissue samples relative to controls.

These data were compared with previously published differential gene expression data from inguinal WAT of cold-exposed mice (GSE13432),[33] an established model of experimental adipose tissue browning (Figure 4B). Our comparison revealed a remarkable trend for concordance despite the differences in species and browning-inducing stimuli: of the 47 factors analyzed in our human samples, 21 were also significantly down-regulated in "browned" adipose tissue from mice relative to controls, and 18 of these were concordant with the factors found to be down-regulated in the pheochromocytoma adipose tissue samples. *Elavl3* and *Elavl4*, the only splicing-related factors significantly up-regulated in browned adipose tissue from human patients, were also up-regulated in mouse BAT, concordantly with findings in human adipose tissue samples. *Hnrnpl* and *Elavl1* were the only identified exceptions to the above-described concordance: they were up-regulated in mice but not in the human pheochromocytoma patient samples.

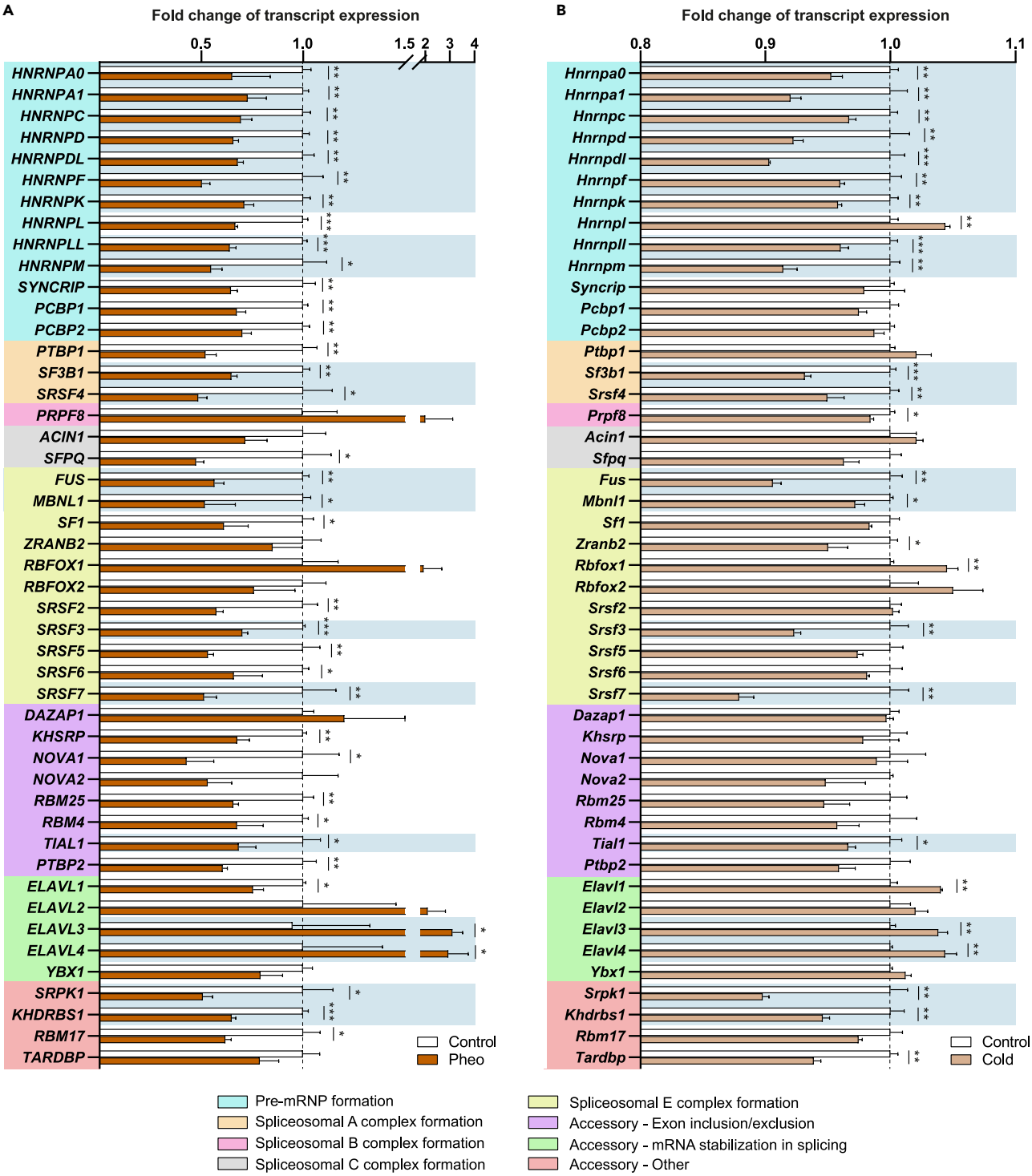

Figure 4. Regulation of splicing factors and splicing-related proteins in association with browning

(A) Transcript levels of splicing factors and splicing-associated proteins in adipose tissue from individuals with pheochromocytoma (brown bars, *N* = 4) and healthy controls (white bars, *N* = 3).

(B) Transcript levels of splicing factors and splicing-associated proteins in mouse inguinal adipose tissue experiencing browning (mice exposed to 4°C for 1 week, beige bars) and controls (mice housed at thermoneutrality, white bars) (*N* = 3 each) (GDS3804, ref. [33]). Data are presented as means ± SEM. *: p<0.05, **: p<0.01, ***: p<0.001 vs. Control; unpaired *t*-test. Blue shading indicates coincidentally-regulated transcripts in humans and mice. Color codes indicate grouping of genes according to their involvement in distinct RNA splicing and processing mechanisms, as indicated at the bottom.

These results support the notion of an overall repression of splicing machinery-associated processes during adipose tissue browning, with a few exceptional upregulations of certain specific RNA-binding proteins involved in splicing regulation.

Cell-autonomous human browning recapitulates the altered gene expression patterns of splicing factors and splicing-related proteins found in adipose tissue from pheochromocytoma patients

To confirm the involvement of regulated splicing in human adipose browning in a cell-autonomous model, we analyzed available transcriptomics datasets obtained from *in vitro* models of differentiating human brown/beige adipocytes. We assessed the expression changes of genes encoding splicing factors and splicing-related proteins in preadipocytes obtained from a 3-month-old Simpson-Golabi-Behmel syndrome patient (SGBS cells), which offer an established model of human brown/beige differentiation,[34] at the non-differentiated stage (day 0) and at early (day 8) and long-term (day 14) stages of browning in cell culture.[35] We also assessed the time courses of transcriptomic changes during the brown adipogenic differentiation of human embryonic stem cells and inducible pluripotent stem cells.[25] This multi-omics comparison revealed that transcripts encoding components involved in forming pre-mRNP and spliceosomal complexes A, B, C, and E, as well as parts of the exon inclusion/exclusion machinery, were generally down-regulated during the *in vitro* differentiation of human cells into brown/beige adipocytes (Figure 5A). There was also a converse upregulation of some components involved in splicing regulation and the mRNA stabilization machinery (e.g., *ELAVL3* and *ELAVL4*) across brown/beige differentiation in the studied cell culture models. These findings were highly concordant with our observations in the browned adipose tissue of pheochromocytoma patients.

To independently validate the results obtained from our GEO datasets analyses, we cultured SGBS cells and used qRT-PCR to assess the transcript levels of several representative components of the splicing machinery at distinct stages of brown/beige adipogenic differentiation (Figure 5B). Our results (Figure 5C) indicated that *HNRNPF* (pre-mRNA formation), *RBFOX2* (spliceosomal E complex), *ELAVL1* (RNA binding/splicing regulation), and *RBM17* (accessory factors in splicing) were down-regulated whereas *ELAVL3* (RNA binding/splicing regulation) was up-regulated, as reported in the cell-based browning databases and seen, with the exception of *RBFOX2*, in browned adipose tissue from our pheochromocytoma patients.

Splicing-driven transcript isoform expression of master regulators of browning and metabolism-related genes is altered in adipose tissue from pheochromocytoma patients

To investigate the potential consequences of altered splicing on gene expression across browning, we compared the expression of transcript isoforms in our adipose tissue RNA-seq data from pheochromocytoma patients versus controls. Our results indicated that 351 isoforms were up-regulated and 452 were down-regulated (Table S1). We next performed a manually curated search of those corresponding to genes known to be involved in adipose tissue metabolism, seeking to identify differential expression of alternative splicing-originated transcript isoforms in browned adipose tissue from pheochromocytoma patients relative to controls (see Table S5 for the number and characteristics of transcript isoforms). The genes showing upregulation of alternative splicing-driven transcripts included *SREBF1* (encoding the transcription factor SREBP-1, which is a master regulator of glucose metabolism and lipogenesis)[36] and several genes encoding proteins involved in the metabolism of lipids (*SLC27A6*, long-chain fatty acid transport protein 6; *PNPLA4*, patatin-like phospholipase A4; *ELOVL6*, fatty acid elongase 6; *ACSDVL*, very long chain acyl-CoA dehydrogenase) and glucose (*PCK1*, cytosolic phosphoenolpyruvate carboxykinase; *ALDOA*, fructose-bisphosphate adolase), as well as *CKMT2*, which encodes the human BAT biomarker, creatine kinase S-type.[22] Figure 6A (top) shows the individual fold-changes for transcript isoforms whose expression levels were significantly higher in pheochromocytoma patients versus controls. Remarkable examples included *CKMT2* and *ALDOA*: The expression levels of the *CKMT2-211* and *ALDOA-205* isoforms were around 15 $\log_2$-fold higher than their control values, whereas the expression levels of the other isoforms of these transcripts were increased around 5 $\log_2$-fold. For *PCK1*, the isoforms *PCK1-204* and *PCK1-205* were induced close to 10 $\log_2$-fold, whereas the other two isoforms were induced close to 5 $\log_2$-fold. The alternative splicing-driven isoform *SREBF1-216* was induced more than 8 $\log_2$-fold. For most of the relevant genes, the differential induction of isoforms involved both protein-coding and non-protein-coding transcripts, with the exception of *ALDOA* and *SLC27A6*, for which only protein-coding transcript isoforms were induced. Regarding the downregulation of alternative splicing-driven isoforms, we analyzed the distinct transcript isoforms encoded by *ANPEP* (alanine aminotransferase), *AOAH* (acyloxyacyl hydrolase),

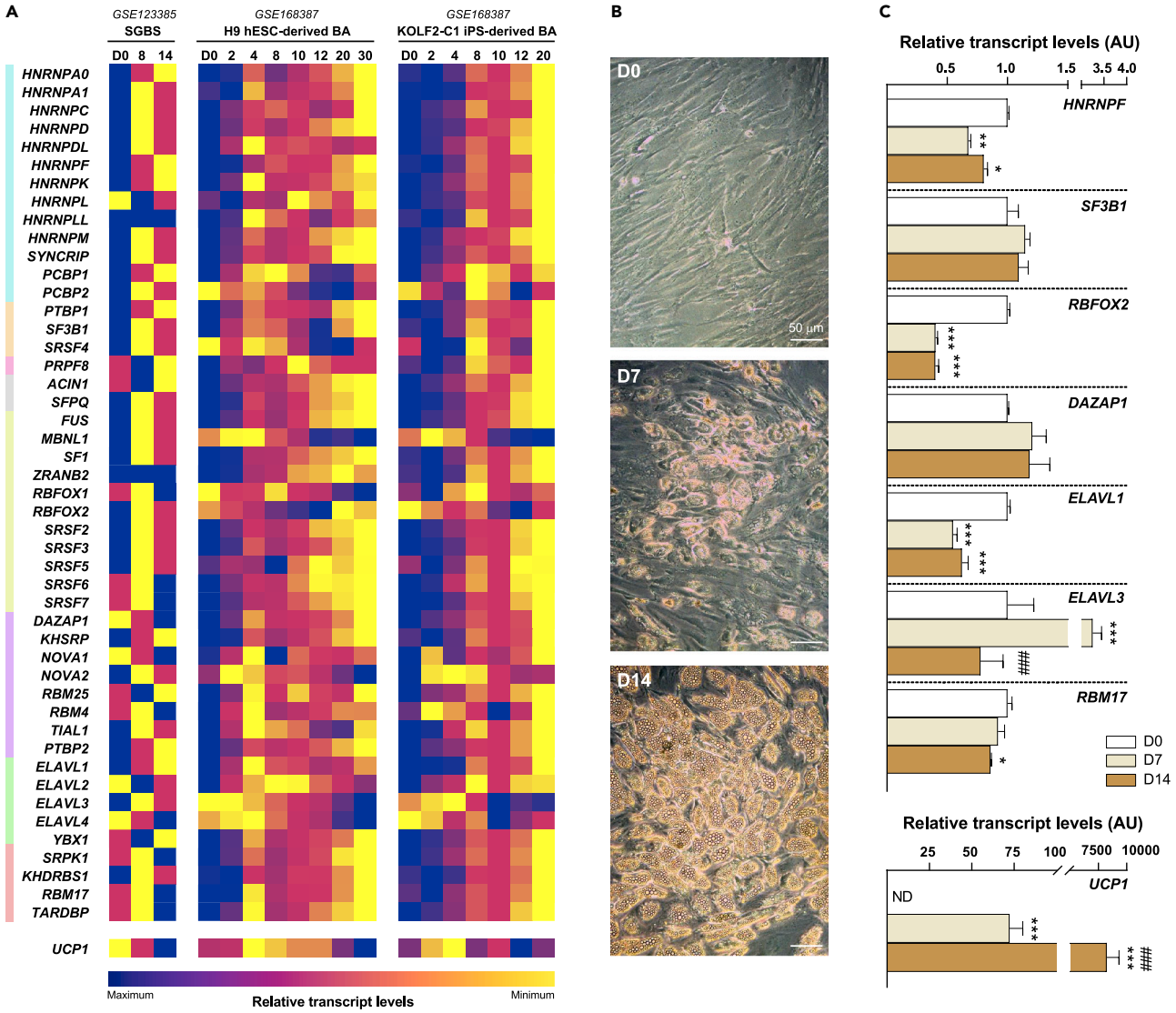

Figure 5. Cell-autonomous regulation of splicing factors and splicing-related proteins in human adipocyte browning

(A) Multitranscriptomics comparison heatmaps of relative levels of transcripts encoding splicing factors and splicing-associated proteins across different days (D) of differentiation into a brown/beige adipocyte (BA) phenotype for three human cell culture models: Simpson-Golabi-Behmel (SGBS) cells, H9 embryonic stem cells (hESC), and KOLF2-C1 inducible pluripotent stem cells (iPS). GEO datasets and color coding (maximum-minimum) are indicated. Expression of *UCP1*, as a marker of BA differentiation, is shown at the bottom.

(B) Representative inverted optical microscopy pictures of SGBS cell cultures at D0 (preadipocytes), D7 (early adipogenic induction), and D14 (fully differentiated beige adipocytes). Scale bars represent 50 µm.

(C) mRNA levels of representative splicing-associated genes and the browning marker *UCP1* in SGBS cells during differentiation at D0, D7, and D14 (n = 3 each). Data are presented as means ± SEM. *: p< 0.05, **: p< 0.01, ***: p< 0.001 vs. D0; ###: p< 0.001 vs. D7; one-way ANOVA followed by Tukey's *post-hoc* test; ND: not detectable.

MTHFD2 (methylenetetrahydrofolate dehydrogenase 2), and *NAMPT* (nicotinamide phosphoribosyltransferase, also known as visfatin) (see Table S5). As seen for upregulation, we observed isoform-specific expression for downregulation (Figure 6A, bottom). This was markedly intense for *NAMPT*/visfatin, whose isoform *NAMPT-202* was more than 10 $\log_2$-fold lower in samples from pheochromocytoma patients versus controls, whereas the other five transcript isoforms were less intensely (5 $\log_2$-fold or less) decreased. Overall, these data indicate that the browning of human adipose tissue is associated with dramatic changes in the alternative splicing-mediated gene expression of metabolic machinery components associated with brown/beige adipocytes.

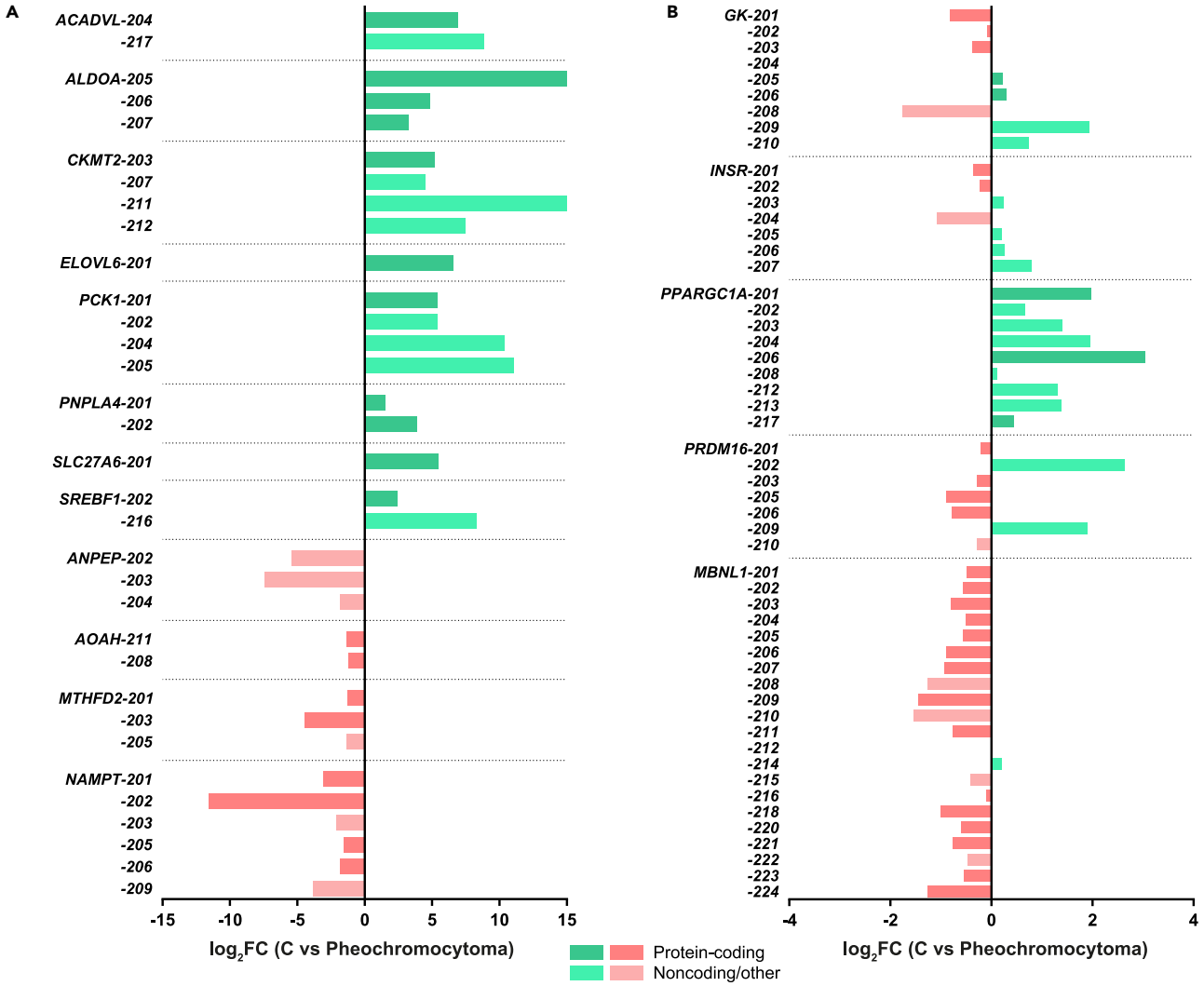

Figure 6. Altered patterns of splicing-driven transcript isoform expression among metabolism-related genes and master regulators of browning in adipose tissue from pheochromocytoma patients

(A) Fold change in expression levels of splicing-driven gene transcript isoforms showing statistically significant upregulation (green positive bars) or downregulation (salmon negative bars) in adipose tissue from pheochromocytoma patients ($N = 4$) relative to controls ($N = 3$).

(B) Fold change in expression levels of detectable transcript isoforms among genes for which splicing-driven isoforms were previously linked to changes in brown/beige adipocyte thermogenic function. Those showing upregulation (green positive bars) or downregulation (salmon negative bars) in adipose tissue from pheochromocytoma patients relative to controls are shown. Darker-colored bars represent protein-coding isoforms. The numbering of the transcript isoforms corresponds to ENSEMBL naming and annotations, based on human genome assembly GRCh38.p14 (hg38) from the Genome Reference Consortium. See also Table S5.

We further analyzed the altered alternative splicing-driven expression of transcript isoforms for genes previously reported to exhibit brown/beige thermogenic function-related alternative splicing in rodent models, including those encoding glycerol kinase (*GK*),[37] insulin receptor (*INSR*),[38] the master transcriptional regulators of thermogenic adipocyte differentiation, *PPARGC1A*[39] and *PRDM16*,[40] and the splicing regulator, muscleblind-like 1 (*MBNL1*).[41] *PPARGC1A* showed a concordant upregulation of distinct transcript isoforms in browned tissue from pheochromocytoma patients (Figure 6B), which was consistent with the above-described bulk transcript level data (Figure 2A); however, upregulation occurred at distinct ranges of intensity according to the isoform (e.g., there was around 3-fold $\log_2$-induction of *PPARGC1-206* isoform but a negligible induction of *PPARGC1A-208*. *MBNL1*, meanwhile, showed consistent downregulation of distinct splicing-mediated transcript isoforms, which also agreed with the bulk data shown in Figure 4A and the overall downregulation of splicing regulators during browning. There was no major

difference in the expression levels of *MBNL-204*(lacking exon 5) relative to isoforms *-201* and *-202* (bearing exon 5) in browned adipose tissue from pheochromocytoma patients, which contrasted with results obtained for equivalent isoforms in a cellular mouse model of brown adipocyte differentiation.[41] The isoform transcript levels for *GK*, *INSR*, and *PRDM16* were distinctly modified in association with browning. For *GK*, some transcript isoforms were markedly up-regulated (e.g., the non-protein encoding isoform *GK-209*) whereas others were intensively down-regulated (e.g., the non-protein encoding *GK-208* and the protein-encoding *GK-201*) in adipose tissue from pheochromocytoma patients. The same was seen for *INSR*, as the non-protein-encoding *INSR-207* isoform was induced whereas *-201* and *-202* (human equivalents: the exon 11-containing and exon 11-lacking transcripts, respectively) were reduced in mice.[38] For *PRDM16*, the two non-protein-encoding transcript isoforms *-209* and *-202* were induced by more than 2 log_2-fold whereas the other isoforms, including protein-encoding ones, were down-regulated. Collectively, these data obtained from pheochromocytoma patients indicate that the browning of human adipose tissue is associated with major changes in the alternative splicing of key master factors controlling the brown/beige adipogenic processes.

DISCUSSION

We herein report the non-biased transcriptomics analysis of adipose tissue from patients with pheochromocytoma. This condition can be used as a model of human adipose tissue browning, and allowed us to identify differential splicing control as strongly associated with the ability of human adipose tissue to acquire a thermogenic brown/beige phenotype.

Our whole-genome gene expression profiling of adipose tissue from pheochromocytoma patients confirmed the intense browning of adipose tissue in the visceral compartment of these individuals. This is believed to reflect chronic exposure to high levels of tumor-secreted norepinephrine, which mimics the sympathetic stimulation of fat to elicit browning. Historically, research on adipose tissue from pheochromocytoma patients led to the discovery that human adipose tissue can express *UCP1* mRNA when acquiring brown fat features.[15] Subsequent studies on cellular morphology,[16] gene expression,[18,20] and uncoupled mitochondrial activity[19] confirmed the appearance of substantial amounts of brown adipocyte-like cells, likely of the beige/brite type, in formerly white fat visceral depots of these patients. Our study establishes in a non-biased manner that this browning process is associated with an overall induction of genes related to enhanced mitochondrial thermogenesis and lipid and carbohydrate catabolic pathways, and an overall reduction of pro-inflammatory pathways. These findings are consistent with existing concepts regarding the phenotypic features of thermogenic adipose tissue.[2,28] In humans, a higher presence of thermogenic cells in visceral relative to subcutaneous fat was suggested years ago on the basis of UCP1 expression,[42] and recent data based on single nuclei transcriptome analysis identified a thermogenic adipocyte cell population in humans only in the visceral depot.[43] Moreover, a case of massive brown adipose tissue infiltration-with functional evidenced of metabolic activity on the basis of PET-scan assays-was reported in the visceral adipose tissue depot in a patient with type 2 diabetes with a catecholamine-secreting paraganglioma,[44] indicating that human visceral adipose tissue holds an unprecedented potential for brown adipogenic differentiation. Overall, the appearance of a large number of adipocytes showing a whole pattern of brown phenotype in omental adipose tissue from patients with pheochromocytoma is consistent with the pre-existent population of thermogenic adipocytes in the visceral adipose compartment.

By using pheochromocytoma-associated browning of adipose tissue in humans as a model, we revealed that splicing-driven processes may be important for browning. The massive downregulation of splicing-related machinery components, with a few up-regulated exceptions, was also found in rodent and human cell-autonomous models of adipocyte browning.

In recent years, the relevance of alternative splicing has been recognized in adipose tissue pathophysiology.[45] Impaired splicing in preadipocytes was recently reported to be essential for pathologically altered preadipocyte differentiation in obesity[46] but the specific role of splicing processes in the program of thermogenic differentiation (i.e., the acquisition of a brown/beige phenotype) is not well understood. Scattered reports in mouse models have indicated that brown adipogenesis is associated with downregulation of the splicing factors and regulators *Ksrp*,[47] *Nova 44½* ,[48] *Sprk1*,[49] and *Acin1*[50]; loss- and gain-of-function experiments supported the notion that these factors repress brown and beige adipogenesis. A recent study in which beige adipogenesis was enhanced *in vitro* by knocking down the long non-coding RNA, *Ctcflos*, found that there was a concomitant and massive induction of splicing machinery components

and splicing regulating factors (44 up-regulated, 9 down-regulated from the 140 analyzed),[51] further supporting the idea that there is an overall reciprocal relationship between the expression of splicing-related factors and the process of brown/beige adipogenesis.

We observed a few but remarkable exceptions to this relationship, such as *ELAVL3* and *ELAVL4*, which were positively associated with browning. These genes encode members of the ELAVL family of RNA-binding proteins (also called Hu proteins), which are known to stabilize mRNAs and control alternative splicing to regulate gene expression.[52] *Elavl1* has been reported to act as a negative regulator of WAT browning in rodent models,[53] which is consistent with our observation that it is down-regulated in BAT from pheochromocytoma patients and in cellular models of human brown/beige adipogenesis. Other studies have indicated that ELAVL3 and ELAVL4 are involved in alternative splicing during neural development[54,55] and ELAVL3 is involved in the control of endocrine pancreatic function,[56,57] but their role in adipogenesis is unknown. The expression of these splicing regulators was found to be up-regulated in association with browning in pheochromocytoma patients, in rodent models of adipose browning *in vivo*, and in human cell models of brown adipogenic differentiation *in vitro*. Further research is warranted to explore the potential positive impact of these ELAVL family members on brown/beige adipocyte gene expression via the control of alternative splicing processes.

Our data reveal that altered splicing is substantially associated with the pattern of transcript isoforms expressed during human adipose browning, especially for molecular regulators of lipid and carbohydrate metabolism. Thus, we speculate that alternative splicing processes are involved in remodeling adipose tissue enzymatic properties toward the metabolic and thermogenic features characteristic of human brown/beige adipose tissue. Moreover, previous candidate-driven studies in rodent models recognized that genes encoding master factors involved in the control of browning, such as PRDM16[40] and InsR,[38] are expressed differentially because of alternative splicing-driven mechanisms, leading to the synthesis of protein isoforms that distinctly control adipose thermogenic functions. Our data support that browning in humans is also associated with a re-arrangement of alternative splicing-driven transcript isoforms encoding PRDM16 and InsR. Although browning in patients with pheochromocytoma did not increase *InsR* and *PRDM16* global expression, there is a trend to increased InsR-A (*INSR-202*)/InsR-B (*INSR-201*) isoform ratio, and PRDM16-exon16 (*PRDM16-206*)/PRDN16+exon16 (*PRDM16-201*) in adipose tissue from patients relative to controls, concordantly with the behavior of these isoforms described in experimental brown adipocyte differentiation models.[38,40] Moreover, other critical enzymatic factors involved in the specialized metabolic machinery of thermogenic brown/beige adipocytes (as shown in Figure 6) are strongly affected by alternative splicing-driven differential expression of isoforms during human adipose tissue browning.

Collectively, our data suggest that the splicing process modifications associated with a browned phenotype of adipose cells may act via direct modification of the enzymatic machinery involved in metabolic and thermogenic functions and/or more indirectly by affecting the isoform expression patterns of master regulators of browning, which would then induce the enzymatic machinery of brown/beige adipocytes.

Recent years have witnessed intense developments in drug design efforts to modify splicing as a potential tool for treating cancer and other diseases.[58] Here, we demonstrate that splicing may play an important role in human adipose browning. Further research is warranted to explore whether splicing-modifying drugs could be used to target and promote the browning of thermogenic adipose tissue to improve obesity and associated diseases.

Limitations of the study

The current study has several limitations to be considered. The analysis of adipose tissue in pheochromocytoma patients has been used for decades as a model of human adipose browning in response to adrenergic stimulation, in light of the intrinsic difficulties of intervention strategies to address adipose tissue browning in humans. However, pheochromocytoma is ultimately a pathological condition, and the events associated with the acquisition of a brown/beige phenotype in adipose tissue found in patients cannot be ruled out to involve pathogenic-related signaling, distinct from the actual physiological events controlling human adipose tissue browning. Other issues include relatively small sample size and potential variability over patients' clinical features, and a lack of functional studies that allow one to establish cause-and-effect conclusions regarding the role of alternative splicing. Moreover, the present results should be considered within the context of the high complexity and intricacy of splicing processes, with dozens of splicing factors

and regulators involved, which makes unfeasible in practical terms a comprehensive experimental targeting of each for determining functional consequences. However, the current study can help to prioritize selected sets of molecular actors related to the control of splicing to undertake gain- and loss-of-function experimental approaches to determine their precise role on human adipose browning.

STAR★METHODS

Detailed methods are provided in the online version of this paper and include the following:

- KEY RESOURCES TABLE
- RESOURCE AVAILABILITY
  - Lead contact
  - Materials availability
  - Data and code availability
- EXPERIMENTAL MODEL AND STUDY PARTICIPANT DETAILS
  - Adipose biopsies and processing
  - SGBS cell culture
- METHOD DETAILS
  - RNA isolation and RNA-sequencing
  - Analysis of correlation with *UCP1* expression
  - Functional enrichment analysis
  - Comparative omics analyses
  - RT-qPCR
- QUANTIFICATION AND STATISTICAL ANALYSIS

SUPPLEMENTAL INFORMATION

Supplemental information can be found online at https://doi.org/10.1016/j.isci.2023.106847.

ACKNOWLEDGMENTS

We thank public funding source State Agency of Research (AEI) from the Spanish Ministry of Science (MCIN). Research supported by grant PID2020-114112RB-100 funded by MICIN/AEI/10.13039/501100011033. M.C. is an "Ayudas para contratos predoctorales" researcher (grant PRE2018-085231funded by the MCIN/AEI/10.13039/501100011033 and by by ESF Investing in your future). T.Q. is a "Juan de la Cierva-Incorporación" researcher (grant IJC2020-043380-I funded by the MCIN/AEI/10.13039/501100011033 and by the European Union NextGenerationEU/PRTR). R.C. is a "Juan de la Cierva-Incorporación" researcher (grant IJC2018-037142-I funded by the MCIN/AEI/10.13039/501100011033).

AUTHOR CONTRIBUTIONS

Conceptualization: A.G., P.D., A.V.P., M.G., D.L.E., F.V., and R.C.; Methodology: M.C., A.B.R., M.P., J.V., T.Q.L., A.G.N., and R.C.; Software: F.S., A.P., and R.C.; Formal Analysis: M.C., A.B.R., M.P., A.G.N., S.C., S.F.R., and R.C.; Investigation: M.C., A.B.R., M.P., J.V., T.Q.L., A.G.N., S.F.R., and R.C.; Resources: L.L.P., J.S., A.G., and P.D.; Data Curation: M.C., A.B.R., T.Q.L., A.G.N., F.S., A.P., S.C., S.F.R., and R.C.; Writing – Original Draft Preparation: M.G., F.V., R.C.; Writing – Review and Editing: All authors; Visualization: M.C., A.B.R., and R.C.; Supervision: A.G., P.D., A.V.P., M.G., D.L.E., F.V., and R.C.; Funding acquisition: P.D., M.G., D.L.E., and F.V.

DECLARATION OF INTERESTS

The authors declare no competing interests.

INCLUSION AND DIVERSITY

We support inclusive, diverse, and equitable conduct of research.

Received: January 12, 2023
Revised: March 31, 2023
Accepted: May 4, 2023
Published: May 9, 2023

REFERENCES

1. Cypess, A.M., and Kahn, C.R. (2010). Brown fat as a therapy for obesity and diabetes. Curr. Opin. Endocrinol. Diabetes Obes. *17*, 143–149. https://doi.org/10.1097/MED.0b013e328337a81f.

2. Giralt, M., and Villarroya, F. (2013). White, brown, beige/brite: different adipose cells for different functions? Endocrinology *154*, 2992–3000. https://doi.org/10.1210/en.2013-1403.

3. Wu, J., Boström, P., Sparks, L.M., Ye, L., Choi, J.H., Giang, A.-H., Khandekar, M., Virtanen, K.A., Nuutila, P., Schaart, G., et al. (2012). Beige adipocytes are a distinct type of thermogenic fat cell in mouse and human. Cell *150*, 366–376. https://doi.org/10.1016/j.cell.2012.05.016.

4. Shabalina, I.G., Petrovic, N., de Jong, J.M.A., Kalinovich, A.V., Cannon, B., and Nedergaard, J. (2013). UCP1 in brite/beige adipose tissue mitochondria is functionally thermogenic. Cell Rep. *5*, 1196–1203. https://doi.org/10.1016/j.celrep.2013.10.044.

5. Kazak, L., Chouchani, E.T., Jedrychowski, M.P., Erickson, B.K., Shinoda, K., Cohen, P., Vetrivelan, R., Lu, G.Z., Laznik-Bogoslavski, D., Hasenfuss, S.C., et al. (2015). A creatine-driven substrate cycle enhances energy expenditure and thermogenesis in beige fat. Cell *163*, 643–655. https://doi.org/10.1016/j.cell.2015.09.035.

6. Cannon, B., and Nedergaard, J. (2004). Brown adipose tissue: function and physiological significance. Physiol. Rev. *84*, 277–359. https://doi.org/10.1152/physrev.00015.2003.

7. Cousin, B., Cinti, S., Morroni, M., Raimbault, S., Ricquier, D., Pénicaud, L., and Casteilla, L. (1992). Occurrence of brown adipocytes in rat white adipose tissue: molecular and morphological characterization. J. Cell Sci. *103*, 931–942. https://doi.org/10.1242/jcs.103.4.931.

8. Bonet, M.L., Oliver, P., and Palou, A. (2013). Pharmacological and nutritional agents promoting browning of white adipose tissue. Biochim. Biophys. Acta *1831*, 969–985. https://doi.org/10.1016/j.bbalip.2012.12.002.

9. Altınova, A.E. (2022). Beige adipocyte as the flame of white adipose tissue: regulation of browning and impact of obesity. J. Clin. Endocrinol. Metab. *107*, e1778–e1788. https://doi.org/10.1210/clinem/dgab921.

10. Betz, M.J., and Enerbäck, S. (2015). Human Brown adipose tissue: what we have learned so far. Diabetes *64*, 2352–2360. https://doi.org/10.2337/db15-0146.

11. Sidossis, L., and Kajimura, S. (2015). Brown and beige fat in humans: thermogenic adipocytes that control energy and glucose homeostasis. J. Clin. Invest. *125*, 478–486. https://doi.org/10.1172/JCI78362.

12. Becher, T., Palanisamy, S., Kramer, D.J., Eljalby, M., Marx, S.J., Wibmer, A.G., Butler, S.D., Jiang, C.S., Vaughan, R., Schöder, H., et al. (2021). Brown adipose tissue is associated with cardiometabolic health. Nat. Med. *27*, 58–65. https://doi.org/10.1038/s41591-020-1126-7.

13. Ricquier, D., Nechad, M., and Mory, G. (1982). Ultrastructural and biochemical characterization of human brown adipose tissue in pheochromocytoma. J. Clin. Endocrinol. Metab. *54*, 803–807. https://doi.org/10.1210/jcem-54-4-803.

14. Lean, M.E. (1989). Brown adipose tissue in humans. Proc. Nutr. Soc. *48*, 243–256. https://doi.org/10.1079/pns19890036.

15. Bouillaud, F., Villarroya, F., Hentz, E., Raimbault, S., Cassard, A.-M., and Ricquier, D. (1988). Detection of brown adipose tissue uncoupling protein mRNA in adult patients by a human genomic probe. Clin. Sci. *75*, 21–27. https://doi.org/10.1042/cs0750021.

16. Frontini, A., Vitali, A., Perugini, J., Murano, I., Romiti, C., Ricquier, D., Guerrieri, M., and Cinti, S. (2013). White-to-brown transdifferentiation of omental adipocytes in patients affected by pheochromocytoma. Biochim. Biophys. Acta *1831*, 950–959. https://doi.org/10.1016/j.bbalip.2013.02.005.

17. Di Franco, A., Guasti, D., Mazzanti, B., Ercolino, T., Francalanci, M., Nesi, G., Bani, D., Forti, G., Mannelli, M., Valeri, A., and Luconi, M. (2014). Dissecting the origin of inducible brown fat in adult humans through a novel adipose stem cell model from adipose tissue surrounding pheochromocytoma. J. Clin. Endocrinol. Metab. *99*, E1903–E1912. https://doi.org/10.1210/jc.2014-1431.

18. Hondares, E., Gallego-Escuredo, J.M., Flachs, P., Frontini, A., Cereijo, R., Goday, A., Perugini, J., Kopecky, P., Giralt, M., Cinti, S., et al. (2014). Fibroblast growth factor-21 is expressed in neonatal and pheochromocytoma-induced adult human brown adipose tissue. Metabolism *63*, 312–317. https://doi.org/10.1016/j.metabol.2013.11.014.

19. Vergnes, L., Davies, G.R., Lin, J.Y., Yeh, M.W., Livhits, M.J., Harari, A., Symonds, M.E., Sacks, H.S., and Reue, K. (2016). Adipocyte browning and higher mitochondrial function in periadrenal but not SC fat in pheochromocytoma. J. Clin. Endocrinol. Metab. *101*, 4440–4448. https://doi.org/10.1210/jc.2016-2670.

20. Klímová, J., Mráz, M., Kratochvílová, H., Lacinová, Z., Novák, K., Michalský, D., Kvasnička, J., Holaj, R., Haluzíková, D., Doležalová, R.P., et al. (2022). Gene profile of adipose tissue of patients with pheochromocytoma/paraganglioma. Biomedicines *10*, 586. https://doi.org/10.3390/biomedicines10030586.

21. Acín-Perez, R., Petcherski, A., Veliova, M., Benador, I.Y., Assali, E.A., Colleluori, G., Cinti, S., Brownstein, A.J., Baghdasarian, S., Livhits, M.J., et al. (2021). Recruitment and remodeling of peridroplet mitochondria in human adipose tissue. Redox Biol. *46*, 102087. https://doi.org/10.1016/j.redox.2021.102087.

22. Müller, S., Balaz, M., Stefanicka, P., Varga, L., Amri, E.-Z., Ukropec, J., Wollscheid, B., and Wolfrum, C. (2016). Proteomic analysis of human Brown adipose tissue reveals utilization of coupled and uncoupled energy expenditure pathways. Sci. Rep. *6*, 30030. https://doi.org/10.1038/srep30030.

23. Tan, C.Y., Virtue, S., Bidault, G., Dale, M., Hagen, R., Griffin, J.L., and Vidal-Puig, A. (2015). Brown adipose tissue thermogenic capacity is regulated by Elovl6. Cell Rep. *13*, 2039–2047. https://doi.org/10.1016/j.celrep.2015.11.004.

24. Millward, C.A., Desantis, D., Hsieh, C.-W., Heaney, J.D., Pisano, S., Olswang, Y., Reshef, L., Beidelschies, M., Puchowicz, M., and Croniger, C.M. (2010). Phosphoenolpyruvate carboxykinase (Pck1) helps regulate the triglyceride/fatty acid cycle and development of insulin resistance in mice. J. Lipid Res. *51*, 1452–1463. https://doi.org/10.1194/jlr.M005363.

25. Carobbio, S., Guenantin, A.-C., Bahri, M., Rodriguez-Fdez, S., Honig, F., Kamzolas, I., Samuelson, I., Long, K., Awad, S., Lukovic, D., et al. (2021). Unraveling the developmental roadmap toward human Brown AdiposeTissue. Stem Cell Rep. *16*, 1010. https://doi.org/10.1016/j.stemcr.2021.03.009.

26. Perdikari, A., Leparc, G.G., Balaz, M., Pires, N.D., Lidell, M.E., Sun, W., Fernandez-Albert, F., Müller, S., Akchiche, N., Dong, H., et al. (2018). BATLAS: deconvoluting Brown adipose tissue. Cell Rep. *25*, 784–797.e4. https://doi.org/10.1016/j.celrep.2018.09.044.

27. Jespersen, N.Z., Andersen, M.W., Jensen, V.H., Stærkær, T.W., Severinsen, M.C.K., Peijs, L., Soares, R., Forss, I., Andersen, E.S., Hahn, C.H., et al. (2020). Thermogenic genes are blunted whereas brown adipose tissue identity is preserved in human obesity. Preprint at bioRxiv. https://doi.org/10.1101/2020.05.07.082057.

28. Villarroya, F., Cereijo, R., Villarroya, J., Gavaldà-Navarro, A., and Giralt, M. (2018). Toward an understanding of how immune cells control Brown and beige adipobiology. Cell Metab. *27*, 954–961. https://doi.org/10.1016/j.cmet.2018.04.006.

29. Puigserver, P., Wu, Z., Park, C.W., Graves, R., Wright, M., and Spiegelman, B.M. (1998). A cold-inducible coactivator of nuclear receptors linked to adaptive thermogenesis. Cell *92*, 829–839. https://doi.org/10.1016/s0092-8674(00)81410-5.

30. Chondronikola, M., Volpi, E., Børsheim, E., Porter, C., Saraf, M.K., Annamalai, P., Yfanti, C., Chao, T., Wong, D., Shinoda, K., et al. (2016). Brown adipose tissue activation is linked to distinct systemic effects on lipid metabolism in humans. Cell Metab. *23*, 1200–1206. https://doi.org/10.1016/j.cmet.2016.04.029.

31. Giulietti, M., Piva, F., D'Antonio, M., D'Onorio De Meo, P., Paoletti, D., Castrignanò, T., D'Erchia, A.M., Picardi, E., Zambelli, F., Principato, G., et al. (2013). SpliceAid-F: a

database of human splicing factors and their RNA-binding sites. Nucleic Acids Res. *41*, D125–D131. https://doi.org/10.1093/nar/gks997.

32. Lee, S., Wei, L., Zhang, B., Goering, R., Majumdar, S., Wen, J., Taliaferro, J.M., and Lai, E.C. (2021). ELAV/Hu RNA binding proteins determine multiple programs of neural alternative splicing. PLoS Genet. *17*, e1009439. https://doi.org/10.1371/journal.pgen.1009439.

33. Xue, Y., Petrovic, N., Cao, R., Larsson, O., Lim, S., Chen, S., Feldmann, H.M., Liang, Z., Zhu, Z., Nedergaard, J., et al. (2009). Hypoxia-independent angiogenesis in adipose tissues during cold acclimation. Cell Metab. *9*, 99–109. https://doi.org/10.1016/j.cmet.2008.11.009.

34. Yeo, C.R., Agrawal, M., Hoon, S., Shabbir, A., Shrivastava, M.K., Huang, S., Khoo, C.M., Chhay, V., Yassin, M.S., Tai, E.S., et al. (2017). SGBS cells as a model of human adipocyte browning: a comprehensive comparative study with primary human white subcutaneous adipocytes. Sci. Rep. *7*, 4031. https://doi.org/10.1038/s41598-017-04369-2.

35. Kalkhof, S., Krieg, L., Büttner, P., Wabitsch, M., Küntzel, C., Friebe, D., Landgraf, K., Hanschkow, M., Schubert, K., Kiess, W., et al. (2020). In depth quantitative proteomic and transcriptomic characterization of human adipocyte differentiation using the SGBS cell line. Proteomics, e1900405. https://doi.org/10.1002/pmic.201900405.

36. Kim, J.B., and Spiegelman, B.M. (1996). ADD1/SREBP1 promotes adipocyte differentiation and gene expression linked to fatty acid metabolism. Genes Dev. *10*, 1096–1107. https://doi.org/10.1101/gad.10.9.1096.

37. Ohira, R.H., Dipple, K.M., Zhang, Y.-H., and McCabe, E.R.B. (2005). Human and murine glycerol kinase: influence of exon 18 alternative splicing on function. Biochem. Biophys. Res. Commun. *331*, 239–246. https://doi.org/10.1016/j.bbrc.2005.03.143.

38. Entingh, A.J., Taniguchi, C.M., and Kahn, C.R. (2003). Bi-directional regulation of brown fat adipogenesis by the insulin receptor. J. Biol. Chem. *278*, 33377–33383. https://doi.org/10.1074/jbc.M303056200.

39. Zhang, Y., Huypens, P., Adamson, A.W., Chang, J.S., Henagan, T.M., Boudreau, A., Lenard, N.R., Burk, D., Klein, J., Perwitz, N., et al. (2009). Alternative mRNA splicing produces a novel biologically active short isoform of PGC-1alpha. J. Biol. Chem. *284*, 32813–32826. https://doi.org/10.1074/jbc.M109.037556.

40. Chi, Y.-L., and Lin, J.-C. (2018). RBM4a modulates the impact of PRDM16 on development of brown adipocytes through an alternative splicing mechanism. Biochim. Biophys. Acta. Mol. Cell Res. *1865*, 1515–1525. https://doi.org/10.1016/j.bbamcr.2018.08.001.

41. Hung, C.-S., and Lin, J.-C. (2020). Alternatively spliced MBNL1 isoforms exhibit differential influence on enhancing brown adipogenesis. Biochim. Biophys. Acta. Gene Regul. Mech. *1863*, 194437. https://doi.org/10.1016/j.bbagrm.2019.194437.

42. Oberkofler, H., Dallinger, G., Liu, Y.M., Hell, E., Krempler, F., and Patsch, W. (1997). Uncoupling protein gene: quantification of expression levels in adipose tissues of obese and non-obese humans. J. Lipid Res. *38*, 2125–2133. https://doi.org/10.1016/S0022-2275(20)37142-X.

43. Emont, M.P., Jacobs, C., Essene, A.L., Pant, D., Tenen, D., Colleluori, G., Di Vincenzo, A., Jørgensen, A.M., Dashti, H., Stefek, A., et al. (2022). A single-cell atlas of human and mouse white adipose tissue. Nature *603*, 926–933. https://doi.org/10.1038/s41586-022-04518-2.

44. Søndergaard, E., Gormsen, L.C., Christensen, M.H., Pedersen, S.B., Christiansen, P., Nielsen, S., Poulsen, P.L., and Jessen, N. (2015). Chronic adrenergic stimulation induces brown adipose tissue differentiation in visceral adipose tissue. Diabet. Med. *32*, e4–e8. https://doi.org/10.1111/dme.12595.

45. Chao, Y., Jiang, Y., Zhong, M., Wei, K., Hu, C., Qin, Y., Zuo, Y., Yang, L., Shen, Z., and Zou, C. (2021). Regulatory roles and mechanisms of alternative RNA splicing in adipogenesis and human metabolic health. Cell Biosci. *11*, 66. https://doi.org/10.1186/s13578-021-00581-w.

46. Sánchez-Ceinos, J., Guzmán-Ruiz, R., Rangel-Zúñiga, O.A., López-Alcalá, J., Moreno-Caño, E., Del Río-Moreno, M., Romero-Cabrera, J.L., Pérez-Martínez, P., Maymo-Masip, E., Vendrell, J., et al. (2021). Impaired mRNA splicing and proteostasis in preadipocytes in obesity-related metabolic disease. Elife *10*, e65996. https://doi.org/10.7554/eLife.65996.

47. Chou, C.-F., Lin, Y.-Y., Wang, H.-K., Zhu, X., Giovarelli, M., Briata, P., Gherzi, R., Garvey, W.T., and Chen, C.-Y. (2014). KSRP ablation enhances brown fat gene program in white adipose tissue through reduced miR-150 expression. Diabetes *63*, 2949–2961. https://doi.org/10.2337/db13-1901.

48. Vernia, S., Edwards, Y.J., Han, M.S., Cavanagh-Kyros, J., Barrett, T., Kim, J.K., and Davis, R.J. (2016). An alternative splicing program promotes adipose tissue thermogenesis. Elife *5*, e17672. https://doi.org/10.7554/eLife.17672.

49. Lin, J.-C. (2018). Multi-posttranscriptional regulations lessen the repressive effect of SRPK1 on brown adipogenesis. Biochim. Biophys. Acta. Mol. Cell Biol. Lipids *1863*, 503–514. https://doi.org/10.1016/j.bbalip.2018.02.004.

50. Lin, Y.-C., Lu, Y.-H., Lee, Y.-C., Hung, C.-S., and Lin, J.-C. (2020). Altered expressions and splicing profiles of Acin1 transcripts differentially modulate brown adipogenesis through an alternative splicing mechanism. Biochim. Biophys. Acta. Gene Regul. Mech. *1863*, 194601. https://doi.org/10.1016/j.bbagrm.2020.194601.

51. Bast-Habersbrunner, A., Kiefer, C., Weber, P., Fromme, T., Schießl, A., Schwalie, P.C., Deplancke, B., Li, Y., and Klingenspor, M. (2021). LncRNA Ctcflos orchestrates transcription and alternative splicing in thermogenic adipogenesis. EMBO Rep. *22*, e51289. https://doi.org/10.15252/embr.202051289.

52. Hinman, M.N., and Lou, H. (2008). Diverse molecular functions of Hu proteins. Cell. Mol. Life Sci. *65*, 3168–3181. https://doi.org/10.1007/s00018-008-8252-6.

53. Siang, D.T.C., Lim, Y.C., Kyaw, A.M.M., Win, K.N., Chia, S.Y., Degirmenci, U., Hu, X., Tan, B.C., Walet, A.C.E., Sun, L., and Xu, D. (2020). The RNA-binding protein HuR is a negative regulator in adipogenesis. Nat. Commun. *11*, 213. https://doi.org/10.1038/s41467-019-14001-8.

54. Ogawa, Y., Yamaguchi, J., Yano, M., Uchiyama, Y., and Okano, H.J. (2018). Elavl3 regulates neuronal polarity through the alternative splicing of an embryo-specific exon in AnkyrinG. Neurosci. Res. *135*, 13–20. https://doi.org/10.1016/j.neures.2018.03.008.

55. Sena, R.M., Twiss, J.L., Gardiner, A.S., Dell'Orco, M., Linsenbardt, D.N., and Perrone-Bizzozero, N.I. (2021). The RNA-binding protein HuD regulates alternative splicing and alternative polyadenylation in the mouse neocortex. Molecules *26*, 2836. https://doi.org/10.3390/molecules26102836.

56. Ahn, S., Tak, H., Kang, H., Ryu, S., Jeong, S.M., Kim, W., and Lee, E.K. (2020). The RNA-binding protein, HuD regulates proglucagon biosynthesis in pancreatic α cells. Biochem. Biophys. Res. Commun. *530*, 266–272. https://doi.org/10.1016/j.bbrc.2020.07.022.

57. Kim, C., Lee, H., Kang, H., Shin, J.J., Tak, H., Kim, W., Gorospe, M., and Lee, E.K. (2016). RNA-binding protein HuD reduces triglyceride production in pancreatic β cells by enhancing the expression of insulin-induced gene 1. Biochim. Biophys. Acta *1859*, 675–685. https://doi.org/10.1016/j.bbagrm.2016.02.017.

58. Black, A.J., Gamarra, J.R., and Giudice, J. (2019). More than a messenger: alternative splicing as a therapeutic target. Biochim. Biophys. Acta. Gene Regul. Mech. *1862*, 194395. https://doi.org/10.1016/j.bbagrm.2019.06.006.

59. Harrow, J., Frankish, A., Gonzalez, J.M., Tapanari, E., Diekhans, M., Kokocinski, F., Aken, B.L., Barrell, D., Zadissa, A., Searle, S., et al. (2012). GENCODE: the reference human genome annotation for the ENCODE Project. Genome Res. *22*, 1760–1774. https://doi.org/10.1101/gr.135350.111.

60. Patro, R., Duggal, G., Love, M.I., Irizarry, R.A., and Kingsford, C. (2017). Salmon provides fast and bias-aware quantification of transcript expression. Nat. Methods *14*,

417–419. https://doi.org/10.1038/nmeth.4197.

61. Love, M.I., Huber, W., and Anders, S. (2014). Moderated estimation of fold change and dispersion for RNA-seq data with DESeq2. Genome Biol. *15*, 550. https://doi.org/10.1186/s13059-014-0550-8.

62. Raudvere, U., Kolberg, L., Kuzmin, I., Arak, T., Adler, P., Peterson, H., and Vilo, J. (2019). g:Profiler: a web server for functional enrichment analysis and conversions of gene lists (2019 update). Nucleic Acids Res. *47*, W191–W198. https://doi.org/10.1093/nar/gkz369.

63. Wabitsch, M., Brenner, R.E., Melzner, I., Braun, M., Möller, P., Heinze, E., Debatin, K.M., and Hauner, H. (2001). Characterization of a human preadipocyte cell strain with high capacity for adipose differentiation. Int. J. Obes. Relat. Metab. Disord. *25*, 8–15. https://doi.org/10.1038/sj.ijo.0801520.

64. Quesada-López, T., Cereijo, R., Turatsinze, J.-V., Planavila, A., Cairó, M., Gavaldà-Navarro, A., Peyrou, M., Moure, R., Iglesias, R., Giralt, M., et al. (2016). The lipid sensor GPR120 promotes brown fat activation and FGF21 release from adipocytes. Nat. Commun. *7*, 13479. https://doi.org/10.1038/ncomms13479.

65. Eizirik, D.L., Sammeth, M., Bouckenooghe, T., Bottu, G., Sisino, G., Igoillo-Esteve, M., Ortis, F., Santin, I., Colli, M.L., Barthson, J., et al. (2012). The human pancreatic islet transcriptome: expression of candidate genes for type 1 diabetes and the impact of pro-inflammatory cytokines. PLoS Genet. *8*, e1002552. https://doi.org/10.1371/journal.pgen.1002552.

66. Cnop, M., Abdulkarim, B., Bottu, G., Cunha, D.A., Igoillo-Esteve, M., Masini, M., Turatsinze, J.-V., Griebel, T., Villate, O., Santin, I., et al. (2014). RNA sequencing identifies dysregulation of the human pancreatic islet transcriptome by the saturated fatty acid palmitate. Diabetes *63*, 1978–1993. https://doi.org/10.2337/db13-1383.

STAR★METHODS

KEY RESOURCES TABLE

REAGENT or RESOURCE	SOURCE	IDENTIFIER
Biological samples		
Human omental adipose tissue biopsies	Hospital del Mar; Hospital de la Santa Creu i Sant Pau (Barcelona)	https://www.parcdesalutmar.cat/en/hospitals/hospital-del-mar/; https://www.santpau.cat/en/web/public
Chemicals, peptides, and recombinant proteins		
Dulbecco's Modified Eagle's Medium (DMEM):F-12	Thermo Fisher Scientific	Cat#SCM162
Fetal Bovine Serum (FBS)	Thermo Fisher Scientific	Cat#F7524
Critical commercial assays		
Spurr Low Viscosity Embedding Kit	Merck	Cat#EM0300-1KT
TaqMan™ Reverse Transcription Reagents	Thermo Fisher Scientific	Cat#N8080234
Platinum™ Quantitative PCR SuperMix-UDG w/ROX	Thermo Fisher Scientific	Cat#11743500
NucleoSpin® RNA	Macherey-Nagel	Cat#740955.250
Deposited data		
Unprocessed RNA-sequencing data	This paper; Zenodo	https://doi.org/10.5281/zenodo.7314338
Human reference genome GENCODE build 38, GRCh38.p12	Harrow et al.[59]	RRID: SCR_01496; https://www.gencodegenes.org
Raw RNA-Sequencing data – Cold-exposed mice	Xue et al.[33]	GEO: GSE13432
Raw microarray data – SGBS cells	Kalkhof et al.[35]	GEO: GSE123385
Raw RNA-Sequencing data – H9 hESC and KOLF2-C1 iPS	Carobbio et al.[25]	GEO: GSE168387
Experimental models: Cell lines		
Human: Simpson-Golabi-Behmel syndrome (SGBS) cells	ATCC	RRID: CVCL_GS28; Cat#ATCC® PCS-210-010
Oligonucleotides		
TaqMan™ gene expression probes (see Table S7 for a complete list)	Thermo Fisher Scientific	See Table S7
Software and algorithms		
FastQC v0.11.8	Babraham Bioinformatics	RRID: SCR_01458; https://www.bioinformatics.babraham.ac.uk/projects/fastqc/
Salmon v1.1.0	Patro et al.[60]	RRID: SCR_017036; https://combine-lab.github.io/salmon/
DESeq2 v1.24.0	Love et al.[61]	RRID: SCR_015687; https://bioconductor.org/packages/release/bioc/html/DESeq2.html
g:Profiler ve108_eg55_p17_9f356ae	Raudvere et al.[62]	RRID: SCR_006809; https://biit.cs.ut.ee/gprofiler/
R v4.2.0	R Project	RRID: SCR_001905; https://www.r-project.org/
RStudio v2022.06.2	Posit	RRID: SCR_000432; https://posit.co/products/open-source/rstudio/

(*Continued on next page*)

Continued

REAGENT or RESOURCE	SOURCE	IDENTIFIER
GraphPad Prism v8.0.1	GraphPad Software	RRID: SCR_002798; https://www.graphpad.com/
Other		
HiSeq 2000 sequencer	Illumina; DNAvision (Brussels)	https://www.illumina.com/
7500 Real-Time PCR System	Thermo Fisher Scientific	Cat#4377354

RESOURCE AVAILABILITY

Lead contact

Further information and requests for resources and reagents should be directed to and will be fulfilled by the lead contact Rubén Cereijo (rcereijo@ub.edu).

Materials availability

This study did not generate new unique reagents.

Data and code availability

- The raw transcriptomics data reported in this study cannot be deposited in a public repository because of private company ownership. To request access, contact DNAVision (Brussels, Belgium; infos@dnavision.be). In addition, unprocessed RNA-sequencing count data have been deposited at Zenodo and are publicly available as of the date of publication. DOI is listed in the key resources table. This paper analyzes existing, publicly available data. These accession numbers for the datasets are listed in the key resources table. All other data reported in this paper will be shared by the lead contact upon request.
- This paper does not report original code.
- Any additional information required to reanalyze the data reported in this paper is available from the lead contact upon request.

EXPERIMENTAL MODEL AND STUDY PARTICIPANT DETAILS

Adipose biopsies and processing

Omental adipose tissue was obtained from patients of Caucasian ethnicity with pheochromocytoma during surgical removal of the tumors ($N = 8$), and from age- and ethnicity-matched control individuals ($N = 4$) on the occasion of minor unrelated surgical procedures, as previously described.[18] The procedures was performed in accordance to the Declaration of Helsinki and approved by the medical ethics committees of the Hospital del Mar and Hospital de la Santa Creu i Sant Pau (Barcelona). Informed consent was also obtained from all individuals; the characteristics of those whose samples were used for RNA-seq analysis are shown in Table S6. Upon extraction, biopsies were immediately rinsed with sterile saline and snap-frozen in liquid nitrogen. Frozen biopsies were stored at −80°C until RNA isolation. For biopsies from individuals with pheochromocytoma, prior to freezing, a ~50 mg fragment was isolated *in situ* with a sterile scalpel, fixed in 2.5% glutaraldehyde and 2% paraformaldehyde in 0.1 M phosphate buffer (pH 7.4), and postfixed in 1% osmium tetroxide and 0.8% FeCNK in phosphate buffer. After dehydration in a graded acetone series, tissue samples were embedded in Spurr resin (Merck, Darmstadt, Germany). Ultrathin sections were stained with uranyl acetate and lead citrate and examined by transmission electron microscopy (JEOL 1010, Izasa Scientific, L'Hospitalet deLlobregat, Spain).

SGBS cell culture

SGBS preadipocytes (ATCC Cat# PCS-210-010, RRID:CVCL_GS28) were cultured as previously described.[34,63] Briefly, SGBS cells were maintained in Dulbecco's modified Eagle's medium (DMEM):F12 medium (Thermo Fisher Scientific, Waltham, MA, USA) plus 10% fetal bovine serum (FBS; Thermo Fisher Scientific). When cultures reached confluence, adipogenic differentiation was induced by incubation for 7 days in FBS-free medium containing 20nM insulin, 0.2nM triiodothyronine, 100nM cortisol, 25nM dexamethasone, 500 μM 3-isobutyl-1-methyl-xanthine, and 2 μM rosiglitazone (Merck, Darmstadt, Germany). The cells were then switched to DMEM:F12 plus 20nM insulin, 0.2nM triiodothyronine, and 100nM cortisol,

and maintained for up to 14 days, during which time more than 90% of the cells acquired a fully-differentiated multilocular adipocyte morphology. The utilized cell culture reagents were obtained from Sigma. For the time-course differentiation analyses, SGBS cells at the preadipocyte (D0), shortly after adipogenic induction (D7), and fully differentiated (D14) stages were used. For each time point (n = 3) inverted optic microscopy pictures were taken to visually monitor differentiation, and cells were harvested by removal of medium followed by scraping and RNA extraction was performed as described above.

METHOD DETAILS

RNA isolation and RNA-sequencing

Tissue fragments (~150 mg) of adipose biopsies from controls and pheochromocytoma patients were homogenized using a metal bead-based mechanical procedure in a TissueLyser (QIAGEN, Düsseldorf, Germany). Total RNA was isolated from tissue homogenates using a NucleoSpin RNA kit (Macherey-Nagel, Dueren, Germany) following the manufacturer's protocol. mRNA was purified from 2μg of total RNA using oligo-dT beads; it was then fragmented, retrotranscribed with random primers, and subjected to second-strand synthesis to create double-stranded cDNA fragments. Adaptor ligation, purification of 200-base pair cDNA fragments, amplification of the purified fragments, and library preparation were performed as previously reported by our laboratory.[64] Before sequencing, the RNA integrity number (RIN) of each sample was determined using an Agilent Bioanalyzer 2100; samples with RIN $\geq$ 7.5 were used for RNA-sequencing. The cDNA library quality and quantity were further analyzed as previously described.[64] Libraries yielding satisfactory results were sequenced on an Illumina HiSeq 2000 sequencer (DNAvision, Charleroi, Belgium). The average reads per sample was 45 million; this level of coverage was previously shown to provide sufficient sequencing depth for gene expression quantification and transcript detection.[65,66] Quality control of reads was performed using FastQC (version 0.11.8; bioinformatics.babraham.ac.uk/projects/fastqc). Gene expression was quantified in TPM units (transcripts per million) using Salmon version 1.1.0[60] with the additional parameters "– seqBias – gcBias – validateMappings". GENCODE version 31 (GRCh38.p12) was used as the reference genome[59] and indexed using default parameters; this resulted in 175,775 transcripts corresponding to 35,183 genes. Raw count datasets for each gene and individual transcript expression are available at the Zenodo repository (CERN Data Center, Geneva, Switzerland; see "data and code availability" section). Differential expression analysis between control and pheochromocytoma adipose samples was conducted using DESeq2 version 1.24.0.[61] For each gene and transcript isoform, $\log_2$ fold change ($\log_2$(FC)) values were calculated, and the unpaired Wald test was used to evaluate differential expression. A gene was considered to be differentially expressed between the groups when it met the criteria of $\log_2$(FC) > |0.585| (i.e., FC = |1.5|) and adjusted *p*-value < 0.05 with Benjamini-Hochberg correction.

Analysis of correlation with *UCP1* expression

Expression values of *UCP1* were retrieved from the generated RNA-seq datasets and Pearson's correlation analyses were performed against the levels of all other detected transcripts using R 4.2.0. The threshold for statistically significant correlation was set at $p < 0.05$, yielding r values > |0.70|.

Functional enrichment analysis

Lists of genes that were differentially expressed between control and pheochromocytoma samples (up- and down-regulated) or significantly correlated with the *UCP1* expression level (positively and negatively) were retrieved and imported into g:Profiler (biit.cs.ut.ee/gprofiler/gost).[62] Functional enrichment analyses to identify relevant KEGG and REACTOME-listed pathways were performed as ordered queries with all known genes; statistical significance was accepted at adjusted pvalue <0.05 (with Benjamini-Hochberg correction). For each pathway, the number of genes detected (intersection size), rich factor (intersection size/number of genes listed for each specific pathway) and pvalues were retrieved in tabular format; the top results for each in terms of size were visualized as scatter bubble plots using R 4.2.0 in R Studio (Boston, MA, USA).

Comparative omics analyses

Transcriptional molecular signatures previously used to define BAT or WAT phenotypes in humans[26,27] were assessed in our dataset. Specific brown- and white-associated scores (B_{score} and W_{score}, respectively) were calculated for each experimental sample. Briefly, normalized expression values (TPM) of each of the 98 BAT-selective and 21 WAT-selective genes listed in Perdikari et al.[26] were retrieved from our RNA-seq data

in each of the 3 control and 4 pheochromocytoma individually. Then, for each individual adipose sample, a summatory or TPM values of all transcripts corresponding to either BAT-selective or WAT-selective genes were separately calculated, resulting in the designated brown (B_{score}) or white (W_{score}) adipose tissue cumulative signature scores. The same approach was conducted using the 20 BAT- and 20 WAT-selective gene lists identified by Jespersen et al.[27] Comparisons of these scores, generation of their ratio between control and pheochromocytoma-derived samples, and correlations among the scores were used to identify the brown or white signature of each sample.

Microarray data from white adipose tissue of cold-exposed (4°C, 1 week) or thermoneutrally-housed (30°C) wild-type C57/Bl6 male mice was retrieved from gene expression omnibus (GEO) dataset GSE13432.[33] Expression levels of selected splicing-associated proteins were calculated as the mean of the detection values for all probes covering the expression of each specific transcript. Values were expressed as the fold change relative to thermoneutrality and significant between-group (cold vs. neutral temperature) differences were identified (two-tailed unpaired *t* test; $p<0.05$).

Transcriptomics data from three *in vitro* models of human brown/beige adipocyte differentiation were also retrieved from GEO: 1) microarray data from SGBS cells at three different stages of differentiation (days 0, 7, and 14; n = 1–2 each; GSE123385)[35]; 2) differentiation time-courseRNA-seq data representing the brown/beige adipogenesis of human embryonic stem cells (H9 hESC, day 0–30; n = 3 each); and 3) differentiation time-course RNA-seq data representing the brown/beige adipogenesis of human inducible pluripotent stem cells (KOLF2-C1 iPS, day 0 to day 25, n = 3 each; GSE168387).[25] Mean expression data of selected transcripts of interest for each time point and model were retrieved, calculated, expressed in terms of fold induction from D0, and represented as heatmaps of relative transcript levels using R.

RT-qPCR

The expression levels of genes of interest were quantified by real-time reverse transcriptase polymerase chain reaction (RT-qPCR). RNA was retrotranscribed into cDNA using 0.5 μg of total RNA, random hexamer primers, and Multiscribe reverse transcriptase (TaqMan Reverse Transcription Reagents; Thermo Fisher Scientific) following the manufacturer's protocol. Platinum Quantitative PCR SuperMix-UDG with ROX reagent (Thermo Fisher Scientific) master mix was used in a final volume of 20 μL containing TaqMan probes specific for each gene (see Table S7), as established by the supplier. RT-qPCR amplification was performed and monitored in an ABI 7500 Real-Time PCR System (Thermo Fisher Scientific). The expression of each target gene was normalized to that of the housekeeping gene, *RPLP0*.

QUANTIFICATION AND STATISTICAL ANALYSIS

The statistical analyses during bioinformatics procedures were performed as described above. PCA was conducted and plotted with the *pca* function of R. Comparisons between two experimental conditions were assessed using two-tailed unpaired Student's *t* tests, as applied using GraphPad Prism 8.0.1 (San Diego, CA, USA), while comparisons among three conditions were performed with one-way analysis of variance (ANOVA) followed by Tukey's *post-hoc* test. Correlation between variables was assessed using Pearson's method, as applied using R or Prism. The threshold of statistical significance for all analyses was set at $p< 0.05$. Unless otherwise specified, all data are presented as means ± statistical error of the mean (SEM).